THE ASTROPHYSICAL JOURNAL, 330:78–90, 1988 July 1

MASSES AND MASS-TO-LIGHT RATIOS FOR EIGHT ELLIPTICAL GALAXIES FROM A TEST OF ANISOTROPIC MODELS

G. BERTIN, R. P. SAGLIA, AND M. STIAVELLI
Scuola Normale Superiore, Pisa
Received 1987 August 3; accepted 1987 December 18

ABSTRACT

A detailed test of the quality of a simple family of anisotropic self-consistent global models (f_∞) for quasi-spherical galaxies is made by considering a set of bright ellipticals with available photometric and kinematical data. The photometric fit, under the assumption of constant mass-to-light ratio, not only proves to be very good (in the majority of cases the residuals are smaller than 0.15 mag), but also better than fits based upon the isotropic King models or the $R^{1/4}$ law. In addition, the fit to the kinematical data allows us to determine total masses and mass-to-light ratios. Seeing convolution effects are also briefly discussed and illustrated. In spite of the relatively small number of cases considered, the present study has the character of a survey; in order to get precise numbers in a specific case we recognize that it would be crucial to undertake a deeper study of the seeing conditions, to incorporate the detailed variation of the photometric error with radius, and, especially, to work on more accurate and extended kinematical data.

Subject headings: galaxies: internal motions — galaxies: photometry — galaxies: structure

I. INTRODUCTION

Ellipticals are collisionless systems that are generally "pressure" supported even when flattened. Their overall three-dimensional symmetry and structure is not known. An important clue to their structure and to their formation is provided by the empirical $R^{1/4}$ *luminosity* law (de Vaucouleurs 1948). The existence of such a law is indicative of a common underlying mass distribution in these systems. The fact that this law is universal suggests that essentially a single physical mechanism characterizes their formation.

From a theoretical point of view an infinite number of ellipsoidal self-consistent stellar dynamical equilibria can be constructed. Certain conjectures on the processes of galaxy formation (i.e., incomplete violent relaxation—see Lynden-Bell 1967; Shu 1978; Stiavelli and Bertin 1987) can restrict the possible options to some extent. On the other hand, a number of observational limitations (especially the fact that relevant data are in the form of projected quantities in a finite radial range and our ignorance on the amount and the distribution of dark matter) prevent us from proposing *unique* dynamical models that incorporate the observed features of a given ellipsoidal stellar system. Therefore not only do we face the problem of understanding *why* the $R^{1/4}$ law is universal, but also that of deciphering *what* it is tracing.

In this context various lines of research have been followed. In one approach astronomers have tried to judge which *empirical* law best represents the luminosity profiles of ellipticals (Kormendy 1977*b*; King 1978; Schweizer 1979). Among the empirical studies we include the tests of the theoretical King (1966) models, since these isotropic equilibria were originally constructed to describe different physical systems. To be sure, King models can provide a reasonable fit to many ellipticals (see also following sections).

In another approach the observed properties, such as the luminosity law, are *imposed*, within a set of simplying assumptions, and then stellar dynamical methods are applied to construct distribution functions that reproduce a given set of data (e.g., Newton and Binney 1984; Merritt 1985; Richstone and Tremaine 1985). These methods can provide precious information on the dynamical implications of the observed luminosity profiles in ellipticals but do not face the issue of the universality of such a law.

Some ellipticals possess a sizeable amount of gas that can be used to trace the gravitational field. For these objects one can try to disentangle empirically the luminosity from the mass profiles (see Raimond *et al.* 1981; van Gorkom *et al.* 1986; Caldwell, Kirshner, and Richstone 1986; Davies and Illingworth 1986; Dressel 1987; Bertola *et al.* 1987). This approach is very interesting but suffers from the fact that the gas may not be in circular motion and often the gas data probe a modest radial range only. In addition, especially if the geometry is obviously nonspherical, this approach is best used to show the inconsistency of certain models rather than to identify the underlying global structure. In passing, we also note that large-scale X-ray emission does not necessarily imply large amounts of dark matter (see Trinchieri, Fabbiano, and Canizares 1986).

In a different line of research (Bertin and Stiavelli 1984, 1987) a simple criterion has been formulated in order to construct stellar dynamical equilibria that are likely to be formed in the process of collisionless collapse (van Albada 1982; Stiavelli and Bertin 1987). From this point of view, dark matter, if present, may have evolved like luminous matter so that a constant mass to light ratio is a natural assumption (so far not contradicted by the observations; see Sancisi and van Albada 1987). These studies have led to equilibrium sequences that are appealing from the theoretical point of view (see remarks by Tremaine 1987), and these turn out to have realistic luminosity profiles as a built-in property. The simplest equilibrium sequence to incorporate these features is the f_∞-distribution function which is the focus of the present paper (see definition in § III*a*).

The main purpose of this paper is to make a detailed quantitative test of the quality of the *global* anisotropic f_∞-models when applied to specific observed galaxies. Given the limitations of these theoretical models we have restricted our attention to a set of galaxies that are not obviously flattened. In our study we concentrate on data available in the literature

(see § II). We show that the f_∞-models not only perform *very well*, but also *better*, when compared to fits based on King models or on a strict application of the $R^{1/4}$ law (see § III). In addition the f_∞-models selected by the photometric fit provide velocity dispersions along the line of sight that can fit the kinematical data. Thus, as a direct by-product of our study, we will measure the astrophysically interesting values of the total mass and of the mass-to-light ratio for each object that is considered (§ IV). In this discussion we try to track the various sources of errors and to estimate these errors in the final numbers. Therefore one goal of this paper is to provide a cautionary note on the values of mass-to-light ratios, since equally reasonable fits can sometimes lead to quite different numbers.

Before starting, a brief comment is in order. The f_∞-models are very simple and have been derived under a set of simple assumptions. Therefore we should not be surprised if they happen to be inadequate to describe all the various phenomena that are found in ellipticals. Still it would be nice if they turn out to provide a simple theoretically supported zeroth-order description of these collisionless stellar systems.

II. THE SET OF GALAXIES AND THE DATA

The set of elliptical galaxies that we consider has been selected under the following criteria: (1) We refer to elliptical galaxies with small ellipticity (E0–E2). This condition is required because the anisotropic f_∞-models that we are going to test refer to quasi-spherical objects. (2) We choose cases for which the surface luminosity distribution $L(R)$ and the velocity dispersion along the line of sight $\sigma(R)$ have already been measured. (3) The set should include objects with a variety of luminosity profiles (for example systems traditionally used as prototypes of $R^{1/4}$ law behavior and prototypes of King's models; see Mihalas and Binney 1981). (4) The luminosity distribution $L(R)$ should cover a sufficiently wide radial range to allow for a *global* test of the anisotropic f_∞-models. Thus eight galaxies have been selected: two E0 (NGC 4636 and NGC 4486; i.e., M87), three E1 (NGC 3379, NGC 4374, and NGC 7626) and three E2 (NGC 4472, NGC 7562, and NGC 7619). Note, however, that isophotes with appreciable ellipticity are found in NGC 7562 and NGC 4636 partly in contrast with the E-type. Data on ellipticity profiles and twisting of isophotes are available in the literature, but these issues will not be addressed in the present paper.

The relevant photometric data are taken from Davis *et al.* (1985, hereafter DC85), de Vaucouleurs and Capaccioli (1979, hereafter DV79), Kent (1984, hereafter KE84), King (1978, hereafter KI78), Kormendy (1977*a*, hereafter KO77), Michard (1985, hereafter MI85), and Young *et al.* (1978, hereafter YW78). The data of DC85 consist of CCD photometries in the R band for NGC 4486 and NGC 3379, extending up to $\sim 150''$ with seeing of $\sim 2''.5$ (FWHM). For NGC 4486 we include the accurate V band CCD photometry of YW78 with $1''$ resolution; however, its limited radial range makes it less interesting for some of the goals of the present paper (see point 4 above). The CCD photometries of NGC 7562, NGC 7619, and NGC 7626 taken from KE84 are in the r band of the *uvgr* system of Thuan and Gunn (1976). These extend up to $\sim 100''$ with a seeing of $\sim 2''.5$ (FWHM). Five of the eight galaxies (NGC 4374, NGC 4472, NGC 4486, NGC 4636, and NGC 7626) were examined in the B band (photographic photometry) by KI78. These data reach the very faint outer regions of the galaxies (2% of the sky level); the seeing varies from $1''.2$ to $3''.5$ (FWHM). The photographic photometry in the G band of NGC 3379, taken from KO77, extends out to $\sim 300''$. Error information on the photometric data is usually missing. For NGC 4374 and NGC 4472, the photographic photometries in the blue band of MI85, which extend up to the 27th magnitude, are provided with the mean errors at various locations. Finally, in order to test the anisotropic f_∞-models on cases of larger radial extent, we have considered the photometry of NGC 3379 presented by DV79. This blue-band luminosity profile, derived from photometric and photoelectric data, covers a range in excess of 11 mag down to $\mu_B = 27.8$ mag arcsec^{-2} ($R = 7'.3$).

We note that in some cases sizeable zero point errors may occur. However, the following analysis is essentially not affected by this kind of errors (see, e.g., comment after eq. [7]).

In Table 1 we list for each galaxy (col. [1]) the type (col. [2]; de Vaucouleurs, de Vaucouleurs, and Corwin 1976), the photometric band (col. [3]), the seeing (FWHM in arcsec, col. [4]) and the source of the photometric data (col. [8]). The numbers in columns (5), (6), and (7) are defined in § III*c*.

TABLE 1

PHOTOMETRIC DATA

Galaxy (1)	Type (2)	Photometric Band (3)	FWHM (4)	N (5)	R_{min} (6)	R_{max} (7)	Source (8)
NGC 3379.....	E1	R	$2''.5$	33	$5''.6$	$158''.5$	DC85
		B	3.0	152	0.04	440.0	DV79
		G	1.4	23	3.2	190.5	KO77
NGC 4374.....	E1	B	3.1	6	10.0	177.8	KI78
		B	2.4	19	5.0	281.8	MI85
NGC 4472.....	E2	B	2.0	8	5.6	316.2	KI78
		B	3.3	17	7.9	316.2	MI85
NGC 4486.....	E0p	R	2.8	31	5.9	137.8	DC85
		B	1.4	9	3.2	316.2	KI78
		V	1.1	29	5.5	79.1	YW78
NGC 4636.....	E0	B	1.4	8	3.2	177.8	KI78
NGC 7562.....	E2	r	2.1	31	5.1	101.5	KE84
NGC 7619.....	E2	r	2.0	27	5.9	85.1	KE84
NGC 7626.....	E1p	r	2.0	29	4.4	85.1	KE84
		B	1.1	7	3.2	100.0	KI78

The corresponding kinematical data are taken from Davies (1981, hereafter DA81), Sargent *et al.* (1978, hereafter SY78) and Schechter and Gunn (1979, hereafter SG79). These authors provide the velocity dispersion along the line of sight as a function of the galactocentric distance by analyzing the stellar absorption spectra with the Fourier Transform method. The velocity dispersions measured by DA81 for NGC 3379, NGC 4374, NGC 4472, and NGC 4636 extend up to $\sim 60''$ from the galactic centers. The kinematical data for NGC 4486 and NGC 3379 taken from SY78 extend up to $\sim 72''$ and up to $\sim 15''$, respectively. For NGC 7562, NGC 7619, and NGC 7626 we consider the velocity dispersion profiles as measured by SG79. We assume that the errors on these data are 20%. These data extend up to $\sim 20''$, but Schechter (1986, private communication) remarks that the outermost points are not fully reliable, in particular for NGC 7626.

Of course, other photometric sources could have been used (see, e.g., Pence and Davoust 1985). Some accurate studies already available in the literature (e.g., Lauer 1985*a*; Young *et al.* 1978) have been given lower priority in this paper because their focus is on the (local) core structure and thus they are less suited for the *global* fit that we are addressing (see, e.g., point (4) above). For example, Lauer's (1985*a*) data, for all the galaxies of our set but M87, extend only to 40″. In addition, we understand that better data, especially kinematical data, will soon be published. For the purpose of the present article we limit our choice to the above described sources, which seem to offer a reasonable starting point.

III. THE FIT

a) Anisotropic f_∞-Models

The *anisotropic* f_∞-models are the simplest family of global self-consistent equilibria that have been constructed for slightly oblate collisionless stellar systems following a physically plausible selection criterion (Bertin and Stiavelli 1984, 1987). In general, the relevant distribution function f_∞ depends on three integrals of the motion. In the spherical limit it reads:

$$\begin{aligned} f_\infty &= A(-E)^{3/2} \exp(-aE - cJ^2/2) \quad \text{if } E \le 0 , \\ &= 0 \qquad\qquad\qquad\qquad\quad \text{if } E > 0 , \end{aligned} \tag{1}$$

where $E = v^2/2 + \Phi$ is the energy per unit mass and J^2 is the specific angular momentum (squared). Two of the three dimensional parameters A, a and c, can be set to fix the physical scales of the galaxy. The *index* $\gamma = (ac/4\pi GA)$ is dimensionless so that equation (1) specifies a one-parameter equilibrium sequence. The gravitational potential Φ is determined self-consistently by integrating the Poisson equation. A global self-consistent f_∞-model is *completely* specified by fixing two scales (such as the total mass M and the half-mass radius r_M) and by the value of the dimensionless central potential $\Psi = -a\Phi(0)$. A detailed discussion of the properties of this equilibrium sequence is given by Stiavelli and Bertin (1985).

In the present work we sample the f_∞ equilibrium sequence by considering 12 spherical models with $2 \le \Psi \le 30$. Models with $\Psi < 2$ present unrealistic features and are presumably unstable. Models with $\Psi > 30$ are probably of theoretical interest only and, in any case, their overall appearance is essentially the same as that of the $\Psi = 30$ model. We note that the models with $\Psi \ge 7$ (that provide the best photometric fits; see § III*c*) are very similar to each other; this situation is in contrast with the properties of the equilibrium sequence of King models (see § III*b*), where rapid changes with C are found in the structure of the models for the parameter regimes of astrophysical interest ($C \approx 2$, see § III*c*).

TABLE 2

GRID OF ANISOTROPIC f_∞-MODELS

Ψ (1)	γ (2)	R_{ef} (3)	M (4)	$\sigma(0)$ (5)
2.0.....	30.0	0.61	7.25	0.42
3.5.....	52.5	0.21	4.32	0.51
4.5.....	40.2	0.15	3.50	0.55
5.2.....	20.0	0.18	3.53	0.57
6.0.....	11.0	0.38	4.25	0.59
7.7.....	14.0	0.60	5.41	0.61
8.8.....	18.0	0.48	5.21	0.63
9.6.....	20.0	0.41	4.99	0.64
12.0.....	20.0	0.35	4.58	0.65
18.0.....	18.4	0.39	4.77	0.65
25.0.....	18.2	0.39	4.75	0.65
30.0.....	18.3	0.41	4.87	0.65

In Table 2 we list for each of the 12 spherical models the value of Ψ (col. [1]), the value of γ (col. [2]), the value of the distance from the center R_{ef} that contains half of the projected mass of the model (col. [3]), the value of the total mass (col. [4]), and the value of the central velocity dispersion projected along the line of sight (col. [5]). All the dimensional quantities are calculated with $a = 2$, $A = 1$ and $G = 1/4\pi$. All the models are constructed by fixing the value of the index γ so that Ψ is determined *a posteriori*. In this paper we will label the models with the value of Ψ approximated to two significant digits, in order not to mislead the reader that we are unnecessarily picky in the choice of our grid. For example the $\Psi = 6$ model is in reality characterized by $\Psi = 5.96$. The most interesting property of the anisotropic f_∞-models is the shape of their projected mass density distribution $\Sigma(R)$ which, for high values of Ψ, follows the $R^{1/4}$ law on a wide radial range. Indeed, Stiavelli and Bertin (1985) showed that the differences $\Delta\mu$ between the magnitudes of the anisotropic f_∞-models $\mu_\infty(R) = -2.5 \log_{10} \Sigma(R)$ and the magnitudes of the $R^{1/4}$ law $\mu_{1/4}$ (de Vaucouleurs 1948) are less than 0.2 over a wide radial range when the $R^{1/4}$ law has effective radius $R_e = R_{ef}$ and $M_e = \mu_{1/4}(R_e) = \mu_\infty(R_{ef})$. Thus, *under the assumption of constant mass-to-luminosity ratio*, these models seem to be good candidates for fitting observed galaxies.

We note here that the anisotropic f_∞-models actually follow the $R^{1/4}$ law even better if R_e and M_e are chosen in the following manner. We require that R_e and M_e minimize the quantity χ^2:

$$\chi^2 = \sum_{R_{\min}}^{R_{\max}} [\mu_\infty(R) - \mu_{1/4}(R)]^2 , \tag{2}$$

where

$$\mu_{1/4}(R) = 8.325(R/R_e)^{1/4} + M_e - 8.325 . \tag{3}$$

The sum in equation (2) extends from $R = R_{\min}$ to $R = R_{\max}$, where $R_{\min}$ and $R_{\max}$ are chosen so as to maximize $(R_{\max} - R_{\min})$ under the constraint $|\Delta\mu| < 0.2$ magnitudes for $R_{\min} \le R \le R_{\max}$ (for example for $\Psi = 7.7$ and $\Psi = 18$ the constraint $|\Delta\mu| < 0.2$ can be verified over 10.04 and 10.06 mag, respectively). We remark that this "best-fit" $R^{1/4}$ law with *two* free parameters R_e and M_e, as is often the case for studies where the accuracy of the $R^{1/4}$ law is tested (see Capaccioli 1984, 1987), does not have the total luminosity of the galaxy (model) when extrapolated to all radii.

Once the parameters of an f_∞-model are chosen, the shape of the velocity dispersion along the line of sight $\sigma(R)$ is completely determined. In general, $\sigma(R)$ decreases monotonically with the projected distance from the center R. The profile is flatter for low $-\Psi$ models.

b) *King Models*

The King models (King 1966), originally elaborated to study collisional spherical stellar systems like globular clusters, have often been applied to fit the photometries of ellipticals (see King 1978) and even to study the cores of giant clusters of galaxies like Coma (see Rood *et al.* 1972). In the present paper, focused on the application of the f_∞-models, we also make a comparison with the King models.

The distribution function of the King models is *isotropic*:

$$f_K = A\{\exp(-\beta E) - \exp(-\beta E_c)\} \quad \text{if } E \le E_c < 0 ,$$
$$= 0 \quad \text{if } E > E_c , \tag{4}$$

where A, β, and E_c are constants. We have computed six equilibrium King models in the range $1.72 \le C \le 2.95$ where $C = \log_{10}(R_t/R_c)$ is the standard concentration parameter (King 1966). At the core radius R_c the projected mass density is one half the value of the central projected density. The quantity R_t is the tidal radius of the model. In this region of parameter space the King models are known to provide a reasonable fit to the photometry of ellipticals.

c) *Fitting Procedure*

The adopted fitting method assumes that the (projected) surface density Σ of the models is proportional to the (projected) surface luminosity $\mathscr{L}$ of the galaxies:

$$\Sigma(R) = (M/L)\mathscr{L}(R) . \tag{5}$$

We set $P = -2.5 \log_{10}(M/L)$. *Here M is expressed in the units of the model* (see § III*a*). The *physical* units are decided only after performing the kinematical fit (see eq. [13]). The photometric fit determines which of the considered equilibrium models has the projected mass distribution that best follows the photometric data of the selected elliptical galaxies. The fit involves two parameters. One of them determines the equilibrium model (the value of Ψ or C) and the other is the scale S (equivalent in arcsec of the unit length of the model).

In the simplest approach, only the photometric data brighter than 26 mag arcsec^{-2} at radial distances larger than two times the FWHM of the seeing are considered in the fit. In this way we can ignore the effects of the convolution with the seeing, that are important in the central galactic regions. In addition, the data that can be seriously affected by sky subtraction are excluded from the fit. Criteria of this kind have been suggested by Binney (1982) and adopted by Capaccioli (1984). In § III*e* the issue of the seeing will be discussed further and so in some cases we will incorporate the innermost photometric data points. In one separate case (NGC 3379 of DV79), where accurate data are available on a large radial extent, we provide a full fit over more than 11 mag. In Table 1, in addition to the quantities defined in § II, we give also the number of data points considered in the fit (col. [5]) and the distance from the center in arcsec of the first (R_{min}) and the last (R_{max}) point considered (cols. [6] and [7]). For NGC 4486, data of YW78, R_{min} has been chosen to be $\sim 5''$ in order to exclude the peculiar structure of the nucleus which cannot be described by the f_∞-models.

The fit over these data is performed by determining the parameters S and Ψ that minimize the value of the quantity

$$\chi^2 = \sum_{R_{min}}^{R_{max}} \{[m(R) - \mu(R/S) + P]/\sigma_m(R)\}^2/(N-2) . \tag{6}$$

In this paper we are trying to provide a quantitative measure of the quality of the fits. We do so by introducing a χ^2-parameter *by analogy* with more standard statistical analyses. For example, we normalize χ^2 to the number of data points N (see Table 1) minus the number of parameters (two in this case), although $(N-2)$ is likely to exceed the actual "number of degrees of freedom" of the fit. In fact, the number of *independent* data points of a given set of photometric data is difficult to estimate. The quantity $m(R)$ is the surface brightness (mag arcsec^{-2}) at distance R from the center of the galaxy, σ_m is the error on the value of m, and μ is the projected mass density of the model. The sum extends from R_{min} to R_{max} (see Table 1). Since most of the photometric sources used in the present paper do not provide error information, for simplicity in our calculations we take $\sigma_m = 0.1$ mag arcsec^{-2} = constant, as a realistic estimate of the *mean* error on the data (see Capaccioli and de Vaucouleurs 1983). (We note that, because of this assumption, the following analysis tends to overestimate the importance of the outer points. The role of the photometric errors in the fit is illustrated later in this section, where the two examples of MI85 are discussed.) The quantity P is an overall scale factor that is *fixed* by imposing that the model has the same total luminosity (up to R_{max}) as the galaxy:

$$\int_0^{R_{max}} \mathscr{L}(R) R\, dR = 10^{(P/2.5)} \int_0^{R_{max}} \Sigma(R/S) R\, dR . \tag{7}$$

We calculated P by direct integration via linear interpolation from the surface luminosity data points. Note that for this purpose we include data points with $R < R_{min}$. Zero point errors in the photometry that is considered would affect the value of P but not the value of S in the fit. Since our estimate of the mass of the galaxy is independent of P (see eq. [13]), zero point errors do not affect the determination of physical quantities in our analysis.

The formal errors $\delta S = (E_{11})^{1/2}$ and $\delta\Psi = (E_{22})^{1/2}$ on S and Ψ, are related to the error matrix $\boldsymbol{E} = 2\boldsymbol{H}^{-1}$

$$H_{ij} = \frac{\partial^2 \hat{\chi}^2}{\partial x_i \partial x_j} , \tag{8}$$

where $x_1 = S$ and $x_2 = \Psi$ and $\hat{\chi}^2 = (N-2)\chi^2$. The actual values of H_{ij} have been determined numerically from equation 6 by evaluating $\hat{\chi}^2$ near its minimum:

$$\hat{\chi}^2(S + \Delta S, \Psi + \Delta\Psi) = \hat{\chi}^2(S, \Psi)$$
$$+ \tfrac{1}{2}(H_{11}\Delta S^2 + 2H_{12}\Delta\Psi\Delta S + H_{22}\Delta\Psi^2) . \tag{8a}$$

In an analogous way we have determined the King models that best fit the photometric data.

We have also fitted the photometric data with the $R^{1/4}$ law by calculating the values of R_e and M_e that minimize the quantity:

$$\chi^2_{1/4} = \sum_{R_{min}}^{R_{max}} \{[m(R) - \mu_{1/4}(R)]/\sigma_m(R)\}^2/(N-2) . \tag{9}$$

As we have already pointed out in § III*a*, this best fit does not have the total luminosity of the galaxy when extrapolated to all radii. Therefore in this approach we are treating the $R^{1/4}$ law

TABLE 3

PHOTOMETRIC FIT

		f_∞			KING			$R^{1/4}$		
GALAXY (1)	SOURCE (2)	$S \pm \delta S$ (3)	$\Psi \pm \delta\Psi$ (4)	$\chi^2 \pm \delta\chi^2$ (5)	$S \pm \delta S$ (6)	$C \pm \delta C$ (7)	χ^2 (8)	R_e (9)	M_e (10)	χ^2 (11)
NGC 3379.....	DC85	150.9 ± 5.1	25.0 ± 5.5	**0.68** ± 0.25	690.1 ± 24.8	2.03 ± 0.4	1.11	52.7	20.5	1.00
	KO77	144.4 ± 12.9	25.0 ± 4.5	**1.05** ± 0.31	656.1 ± 17.6	2.03 ± 0.02	2.78	49.0	21.5	1.62
NGC 4374.....	KI78	241.7 ± 21.0	25.0 ± 7.2	2.06 ± 0.71	1067.0 ± 87.7	2.03 ± 0.07	1.59	79.9	22.9	2.70
	MI85	(281.8 ± 14.6)	(25.0 ± 5.7)	(**0.47** ± 0.34)	(871.5 ± 93.2)	(2.35 ± 0.1)	(0.95)	(97.9)	(23.2)	(0.73)
		264.7 ± 5.7	25.0 ± 2.8	**1.39** ± 0.34	803.9 ± 9.6	2.35 ± 0.01	5.9	87.9	23.0	4.36
NGC 4472.....	KI78	353.9 ± 23.9	25.0 ± 9.1	**0.51** ± 0.58	1199.0 ± 114.2	2.35 ± 0.1	2.63	113.8	22.9	1.61
	MI85	(311.4 ± 17.5)	(25.0 ± 6.2)	(**0.64** ± 0.37)	(946.5 ± 17.8)	(2.35 ± 0.03)	(1.01)	(105.5)	(22.9)	(0.98)
		287.9 ± 4.1	25.0 ± 1.8	**5.3** ± 0.37	876.7 ± 4.4	2.35 ± 0.01	12.2	92.6	22.6	14.45
NGC 4486.....	DC85	392.6 ± 31.0	12.0 ± 0.4	0.26 ± 0.26	632.8 ± 24.8	2.69 ± 0.07	1.23	117.2	21.6	**0.19**
	KI78	535.4 ± 17.9	6.0 ± 0.1	2.46 ± 0.53	1086.7 ± 32.5	2.03 ± 0.04	1.29	88.5	22.1	1.93
	YW78	357.7 ± 19.9	12.0 ± 0.3	0.45 ± 0.27	1339.6 ± 16.8	2.03 ± 0.03	0.63	108.9	22.0	**0.10**
NGC 4636.....	KI78	394.0 ± 29.9	12.0 ± 0.6	**0.48** ± 0.58	1335.7 ± 77.7	2.35 ± 0.06	1.53	111.6	24.4	0.79
NGC 7562.....	KE84	80.5 ± 2.1	9.6 ± 0.2	**0.37** ± 0.26	256.1 ± 9.9	2.35 ± 0.04	0.59	31.8	21.7	0.56
NGC 7619.....	KE84	110.5 ± 4.2	30.0 ± 22.5	**0.53** ± 0.28	517.4 ± 26.9	2.03 ± 0.04	0.57	38.4	21.9	0.75
NGC 7626.....	KE84	164.1 ± 1.5	12.0 ± 4.9	**0.11** ± 0.27	288.8 ± 10.5	2.69 ± 0.4	0.43	48.4	22.4	0.14
	KI78	116.9 ± 9.5	18.0 ± 4.1	**0.48** ± 0.63	570.7 ± 23.7	2.03 ± 0.05	1.35	42.6	23.4	0.60

more generously than the f_∞ or the King models. For completeness, we have also checked that by imposing the further constraint of total integrated luminosity and by performing the fit with only one free parameter (the effective radius R_e), the final minimum values of $\chi^2_{1/4}$ (normalized to the number of points minus one) are slightly higher.

In Table 3 we list the results of all the photometric fits. For each galaxy (col. [1]) and photometric data (col. [2]) we give the values of S and δS (col. [3]), Ψ and $\delta\Psi$ (col. [4]) and the χ^2 with the "statistical standard deviation" from unity defined as $[2/(\text{number of points} - 2)]^{1/2}$ (col. [5]), as derived from the anisotropic f_∞-models. In addition, we list the values of S and δS (col. [6]), C and δC (col. [7]) and the corresponding (normalized) χ^2 (col. [8]), as derived from the King models. Finally, in the right part of the table we give the values of R_e (col. [9]), of M_e (col. [10]) and of the (normalized) χ^2 (col. [11]), as derived from the $R^{1/4}$ law. For uniformity all the values of S, δS and R_e are given with one decimal digit, even if we do not expect it to be significant. For two entries (NGC 4374 and 4472 of MI85), we give the results of two different fits: for each case the first line of numbers in parentheses refers to a fit obtained by taking a constant photometric error of 0.1 mag (as is done for all other entries of the table), while the second line refers to a fit that incorporates the error information provided by MI85. From these two cases we can appreciate the role of the variation with radius of the photometric errors on the fit. In particular we note that taking into account the variation of the photometric errors with radius does not affect the choice of the best-fit f_∞-model. When the photometric errors are incorporated, the values of χ^2 are somewhat higher and the values of S are $\sim 8\%$ smaller than that calculated with a fixed error. The effect of the variation of the scale must be added to the analogous contribution due to the convolution with the seeing (see § III*e*) and could imply that the masses calculated in § III*d* are slightly overestimated.

We now describe the fitting procedure for the kinematical data. This fit has one free parameter; i.e., the central projected velocity dispersion V of the model selected by the photometric data. We calculate V by minimizing the quantity:

$$\chi^2_{\text{kin}} = \Sigma\left[\left(\sigma_{\text{obs}}(R) - \frac{V\sigma_{\text{mod}}(R/S)}{\sigma_{\text{mod}}(0)}\right)\Big/\Delta_{\text{obs}}(R)\right]^2\Big/(N_{\text{kin}} - 1)\,, \tag{10}$$

where σ_{obs} is the measured velocity dispersion, Δ_{obs} the related error, σ_{mod} the projected velocity dispersion predicted by the model and S is the scale selected by the photometric fit. For those galaxies with different photometric sources available, the value of S is taken from the photometric fit to the data that we judge to be more accurate (see Table 4). The quantity χ^2_{kin} is normalized to the number of kinematical data points minus the number of parameters (one in this case). On the interpreta-

TABLE 4

KINEMATICAL FIT

		f_∞				KING				
GALAXY (1)	SOURCE (kin.) (2)	V (km s^{-1}) (3)	δV (km s^{-1}) (4)	ΔV (km s^{-1}) (5)	$\chi^2 \pm \delta\chi^2$ (6)	V (km s^{-1}) (7)	δV (km s^{-1}) (8)	ΔV (km s^{-1}) (9)	χ^2 (10)	SOURCE (Photometric) (11)
NGC 3379.....	DA81	243.8	9.2	1.2	1.1 ± 0.5	202.8	7.7	5.3	2.3	DC85
NGC 4374.....	DA81	335.4	9.4	0.7	1.4 ± 0.5	302.1	8.4	0.3	1.3	MI85
NGC 4472.....	DA81	348.6	10.5	0.5	0.7 ± 0.5	312.0	9.4	0.2	1.0	MI85
NGC 4486.....	SY78	358.3	7.0	2.8	0.6 ± 0.4	336.6	6.5	0.8	0.8	DC85
NGC 4636.....	DA81	241.7	12.5	1.0	0.9 ± 0.6	223.0	11.6	0.1	1.2	KI78
NGC 7562.....	SG79	265.3	17.1	0.7	1.0 ± 0.5	243.7	15.6	0.6	0.7	KE84
NGC 7619.....	SG79	358.5	31.7	17.5	1.4 ± 0.6	294.5	25.8	1.6	0.9	KE84
NGC 7626.....	SG79	401.1	31.1	14.1	1.5 ± 0.6	381.5	29.5	7.9	1.3	KE84

tion of $\chi^2_{\rm kin}$ we could make a cautionary remark similar to the case of χ^2 (see comment after eq. [6]). Therefore we find:

$$V = \sigma_{\rm mod}(0)\,\frac{\Sigma\sigma_{\rm mod}(R/S)\sigma_{\rm obs}(R)/\Delta^2_{\rm obs}(R)}{\Sigma\sigma^2_{\rm mod}(R/S)/\Delta^2_{\rm obs}(R)}\,. \tag{11}$$

The formal statistical error on V is δV, where

$$\delta V^2 = \frac{2}{\partial^2\hat{\chi}^2_{\rm kin}/\partial V^2} = \frac{\sigma^2_{\rm mod}(0)}{\Sigma\sigma^2_{\rm mod}(R/S)/\Delta^2_{\rm obs}(R)}\,, \tag{12}$$

where $\hat{\chi}^2_{\rm kin} = (N_{\rm kin} - 1)\chi^2_{\rm kin}$. We calculate also a "theoretical" error ΔV coming from the errors on S and Ψ. The quantity ΔV is defined as the maximum variation of V when S and Ψ are incremented by $\pm\delta S$ and $\pm\delta\Psi$, respectively. We approximate $\Psi \pm \delta\Psi$ with the nearest value in our grid.

Following the same procedure we calculate the values of V, δV, ΔV, and $\chi^2_{\rm kin}$ for the King models.

In Table 4 for each galaxy (col. [1]) and kinematical source (col. [2]), we list the values of V (col. [3]), δV (col. [4]), ΔV (col. [5]) and $\chi^2_{\rm kin}$, with the "standard deviation" from unity defined as $[2/(\text{number of points} - 1)]^{1/2}$ (col. [6]), as calculated from the anisotropic f_∞-models. Then we give the values of V (col. [7]), δV (col. [8]), ΔV (col. [9]), and $\chi^2_{\rm kin}$ (col. [10]), as calculated from the King models, and the photometric source (col. [11]). As in Table 3, the values of V, δV, and ΔV are given with one decimal digit, even though not physically significant. We note that the kinematical data are also the result of a convolution of the actual velocity dispersion with the instrumental resolution, and then, in principle, we should convolve the velocity dispersion of the models before proceeding with the fit. In practice we ignore these effects. The related corrections should be small, since the errors on the kinematical data are quite large.

In Figure 1 we show for each galaxy the photometric data used in Table 4 with the curves representing the best fit anisotropic f_∞-models (*top frame*), the differences between the two (*middle frame*), and the kinematical data with the best fit theoretical curves (*bottom frame*). In the same format we also show the data for the King model in the case of NGC 4374. In Figure 2 the $R^{1/4}$ law fit in the case of NGC 4486 is displayed.

d) Masses and Mass-to-Light Ratios

The total masses of the galaxies are derived from the masses of the models that we selected with the photometric fit, by scaling the unit length, the velocity, and the gravitational constant in the following way:

$$\frac{M}{M_\odot} = \frac{2.33\times10^5\pi}{4\pi\times3.6\times180}\,M_{\rm mod}\,\frac{V^2}{\sigma^2_{\rm mod}(0)}\,SD$$

$$\approx 90 M_{\rm mod}\,\frac{V^2}{\sigma^2_{\rm mod}(0)}\,SD\,. \tag{13}$$

The central velocity dispersion $\sigma_{\rm mod}(0)$ and the mass $M_{\rm mod}$ of the model have been calculated numerically. Their values for the anisotropic f_∞-models are listed in Table 2. The scale S is derived from the photometric fit (Table 3) and the velocity dispersion V from the kinematical fit (Table 4). The actual galactic distances are discussed in great detail by Lauer (1985*b*). For the present purposes we simply refer to an assumed distance D (in Mpc) that is determined by dividing the recession velocity of the galaxy by $H_0 = 50$ km s^{-1} Mpc^{-1}; in addition NGC 7619 and NGC 7626 are assigned the same (mean) distance and NGC 4636, as a member of the Virgo Cluster, is assigned $D = 20$ Mpc. The recession velocity is referred to the Local Group and is taken from Schechter (1980). The numerical constant in equation (13) involves the conversion factor from arcseconds to radians and the factor 2.33×10^5, which is the value of the inverse of the gravitational constant that is required in order to have M expressed in solar masses.

The formal errors δM on M are calculated from

$$\delta M/M = \delta S/S + \delta M_{\rm mod}/M_{\rm mod} + 2[(\delta V + \Delta V)/V + \delta\sigma_{\rm mod}/\sigma_{\rm mod}]\,, \tag{14}$$

where

$$\delta M_{\rm mod} = |\,M_{\rm mod}(\Psi) - M_{\rm mod}(\Psi \pm \delta\Psi)\,|\,, \tag{14a}$$

$$\delta\sigma_{\rm mod} = |\,\sigma_{\rm mod}(\Psi) - \sigma_{\rm mod}(\Psi \pm \delta\Psi)\,|\,, \tag{14b}$$

and $\sigma_{\rm mod}$ refers to its central value. We evaluate equation (14a) and equation (14b) by approximating $\Psi \pm \delta\Psi$ to the nearest value of the grid.

In order to calculate the M/L_B ratios we refer to the total *blue* luminosities (scaled to our assumed distance) of Lauer (1985*b*), that are corrected for extinction. For NGC 4486 we consider the apparent magnitude from Sandage and Tamman (1981).

In Table 5 for each galaxy (col. [1]) we list the assumed distance (col. [2]), the photometric source (col. [3]), the values of M, $\delta M/M$, and M/L_B, as calculated from the anisotropic

TABLE 5

MASSES AND MASS-TO-LIGHT RATIOS

			f_∞			KING		
GALAXY (1)	DISTANCE (Mpc) (2)	PHOTOMETRIC SOURCE (3)	$M(10^{11}\,M_\odot)$ (4)	$\delta M/M$ (5)	$M/L_B(M_\odot/L_\odot)$ (6)	$M(10^{11}\,M_\odot)$ (7)	$\delta M/M$ (8)	$M/L_B(M_\odot/L_\odot)$ (9)
NGC 3379.....	16	DC85	1.5	0.14	9.0	1.8	0.33	10.8
NGC 4374.....	20	MI85	6.1	0.11	11.9	6.3	0.07	12.4
NGC 4472.....	20	MI85	7.1	0.08	6.3	7.4	0.07	6.5
NGC 4486.....	20	DC85	9.8	0.13	11.1	6.4	0.08	7.2
NGC 4636.....	20	KI78	4.5	0.19	11.7	5.7	0.16	15.0
NGC 7562.....	77	KE84	4.8	0.16	4.6	5.0	0.17	4.8
NGC 7619.....	77	KE84	11.5	0.55	7.3	13.4	0.24	8.5
NGC 7626.....	77	KE84	19.8	0.54	14.4	14.4	0.28	10.5

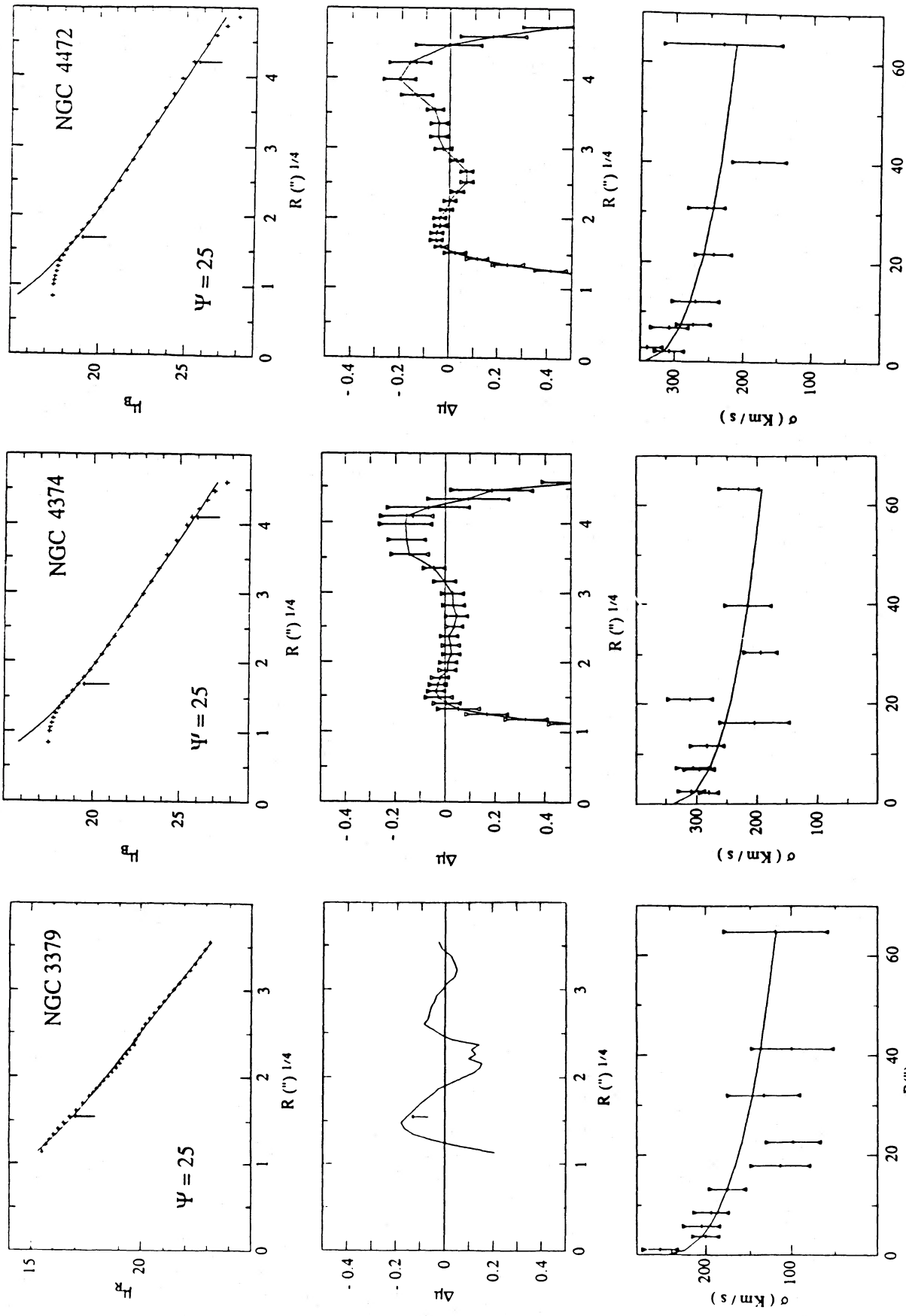

FIG. 1.—For each galaxy (identified on the top right corner) we present three frames. In the top frame we show, as a function of the $\frac{1}{4}$ power of the galactocentric distance in arcsec, the magnitudes μ measured by the authors listed in Table 4 (*crosses*) and the magnitudes μ_∞ of the anisotropic f_∞-model (*solid line*) selected by the photometric fit (see § IIIc). The relevant value of Ψ is indicated on the bottom left corner. In the middle frame the residuals $\Delta\mu = \mu - \mu_\infty$ between the data and the model are shown as a function of the $\frac{1}{4}$ power of the galactocentric distance in arcsec. When $\Delta\mu > 0$ the model is more luminous than the galaxy. Arrows indicate $R_{\min}$ and $R_{\max}$ (see Table 1). When $R_{\max}$ is the last point, the second arrow is omitted. For NGC 4374 and NGC 4472 (of MI85) the photometric data are shown with error bars. In the bottom frame we show, as a function of the galactocentric distance in arcsec, the velocity dispersions along the line of sight in km s^{-1} measured by the authors listed in Table 4 (with error bars) and the projected velocity dispersions of the anisotropic f_∞-model selected by the photometric fit (*solid line*). For NGC 4374 of KI78, as the last column, we show in the same format the fit obtained by the $C = 2.03$ King model.

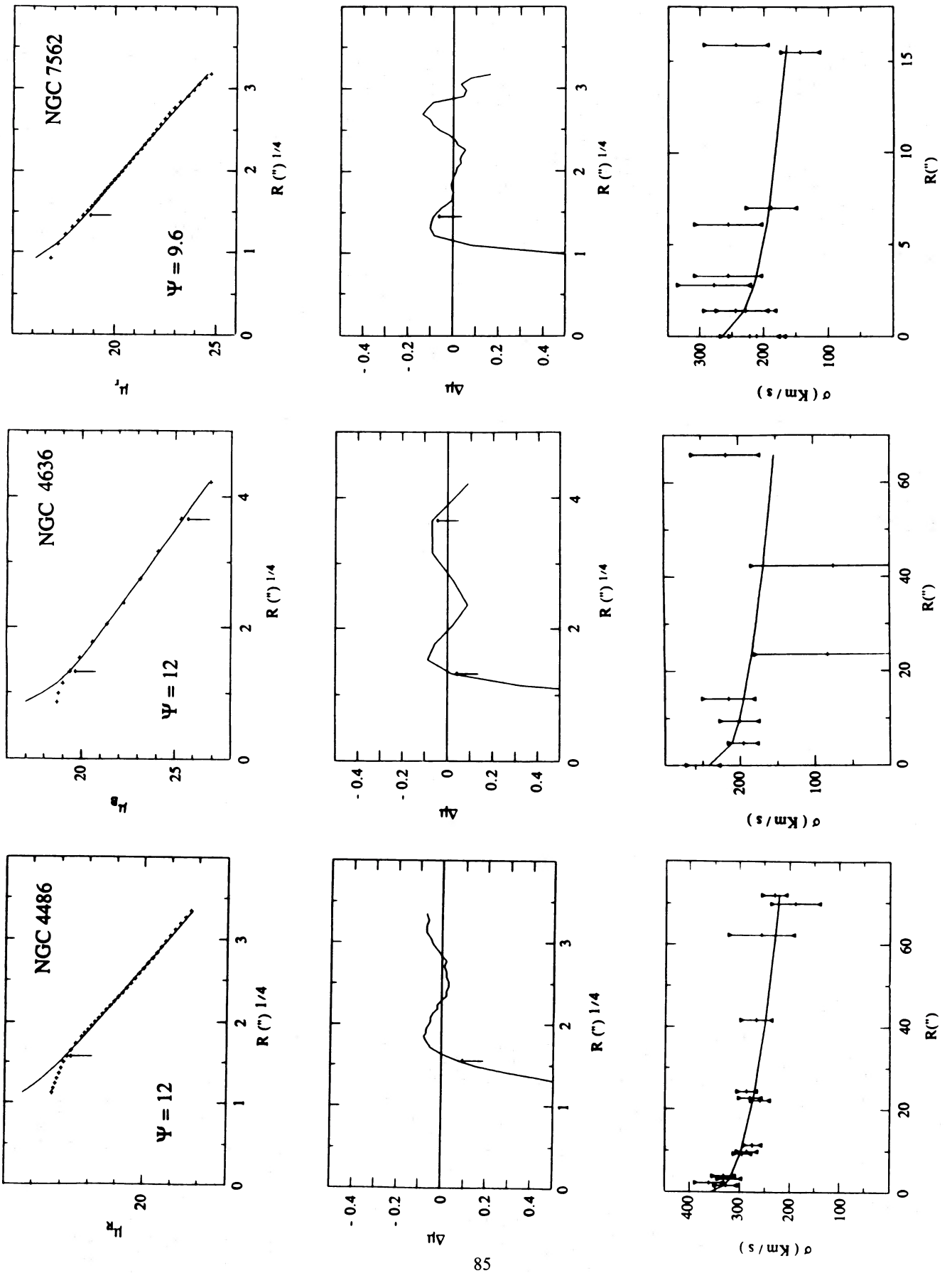

FIG. 1—*Continued*

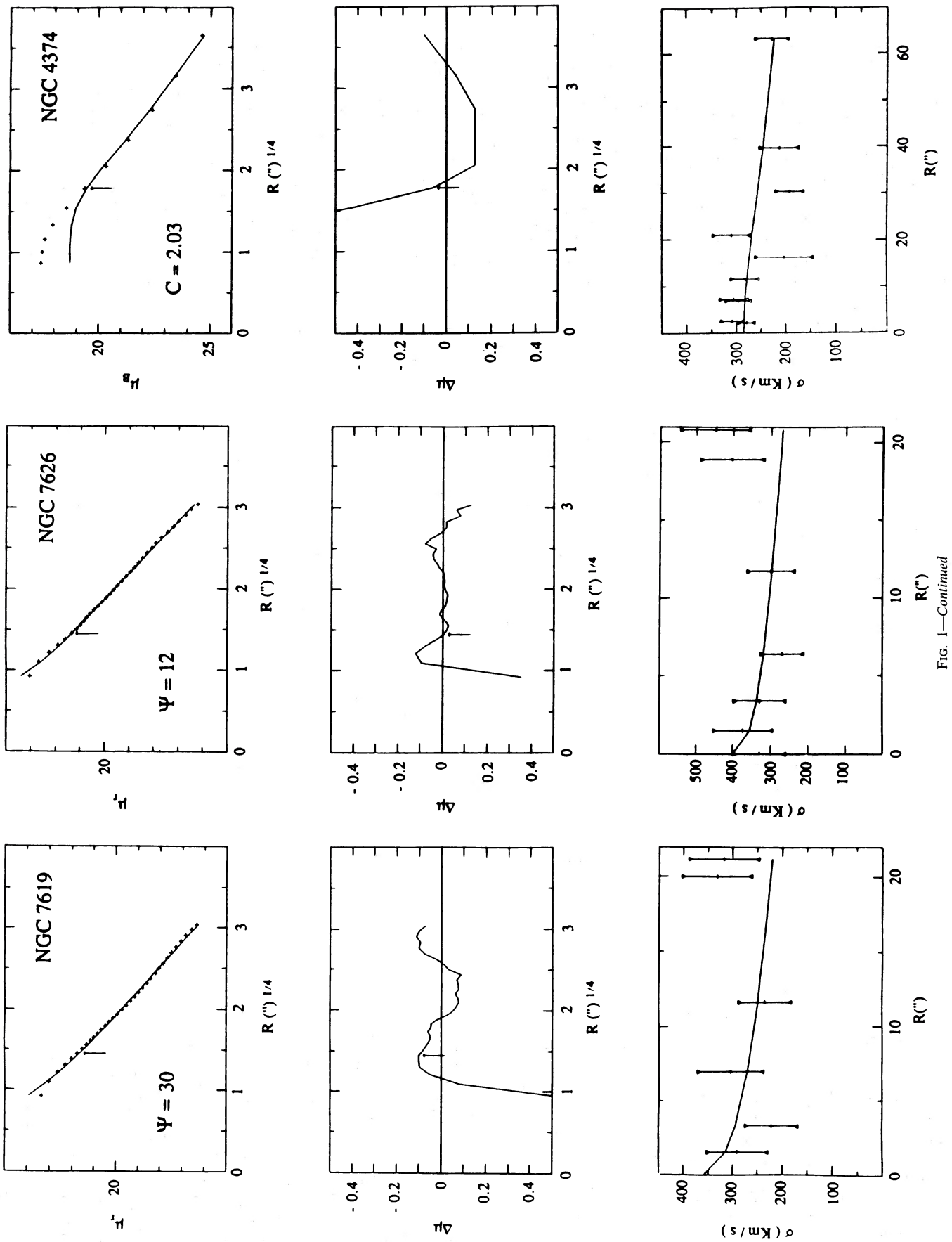

FIG. 1—*Continued*

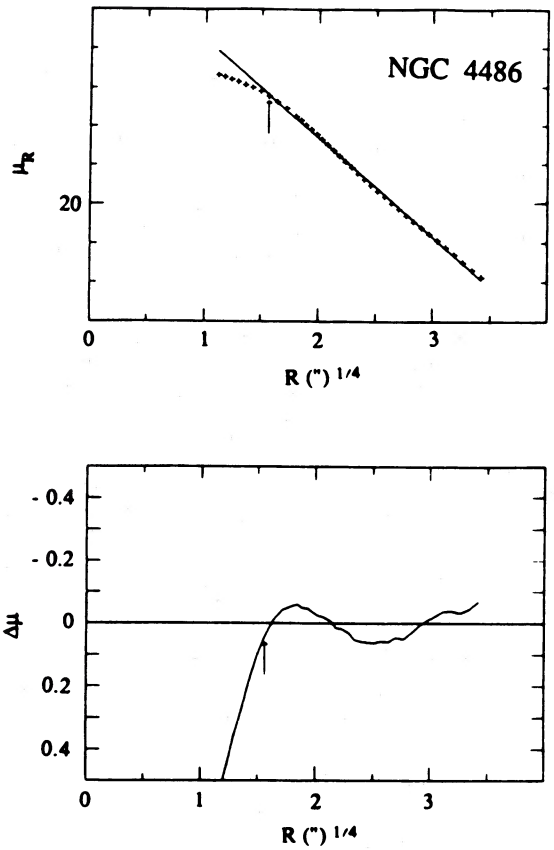

FIG. 2.—For NGC 4486 we show the photometric fit obtained by the $R^{1/4}$ law in a format similar to the upper frames of Fig. 1. For this case the $R^{1/4}$ law performs slightly better than the anisotropic f_∞-models. But the quality of the fit is excellent in both cases. In addition the anisotropic f_∞-models also provide an excellent kinematical fit (see Fig. 1).

f_∞-models (cols. [4]–[6]) and from the King models (cols. [7]–[9]).

The values of the mass-to-light ratios in various frequency bands could also be reconstructed by rescaling the numbers obtained from the quantity P (see eq. [7]) as determined for a given photometry in each fit. For B band photometries this procedure has been checked to give numbers in agreement with those of Table 5. However, we think that the method adopted here gives a more uniform set of M/L_B values and spares us from possible zero points errors in the individual photometries used and from a detailed discussions of other corrections (see Lauer 1985*b*).

e) Seeing

The central regions of the galaxies have been excluded from the simple photometric fit described in § III*c* because they are affected by the seeing. In fact, the measured luminosity $\mathscr{L}^c$ of an object in the sky is related to its real luminosity $\mathscr{L}$ by the convolution with the point spread function (PSF) f, normalized to unity:

$$\mathscr{L}^c(x, y) = \iint \mathscr{L}(x - x', y - y') f(x', y')\, dx'\, dy' , \qquad (15)$$

where (x, y) identify the relevant line of sight.

The PSF can be determined observationally from the luminosity profiles of the stars (King 1971). The discussion of the seeing can be very subtle and in principle it should be carried out by a detailed inspection of the PSF at the time when the photometric data are collected. For general purposes simple approximations are often used. Among the many analytical approximations to the PSF there are Gaussian functions, Gaussian functions with exponential wings, and sums of two or more Gaussian functions (see Schweizer 1979). In the present paper, following Bendinelli *et al.* (1984), we adopt a sum of four Gaussians as our analytical approximation to the PSF:

$$f(R) = \frac{1}{2\pi} \sum_{i=1}^{4} \frac{a_i c_i}{\sigma^2} \exp\left(-\frac{c_i R^2}{2\sigma^2}\right). \qquad (16)$$

Following Bendinelli *et al.* (1984), we take $a_1 = 0.564$, $a_2 = 0.192$, $a_3 = 0.192$, $a_4 = 0.053$, $c_1 = 1$, $c_2 = 0.484$, $c_3 = 0.126$, $c_4 = 0.016$. Using these parameters, the full-width at half maximum (FWHM) of the PSF of equation (16) is 2.52 σ.

In order to complete the study described in this section, we have performed fits with seeing convolution and determined the parameters S and Ψ that minimize the quantity of equation (6), by extending the fit to all the available data points up to R_{max}. The magnitude μ of the convolved model is derived from equation (15) via a linear interpolation. The relevant PSF (eq. [16]) has the FWHM of the seeing reported in the photometric sources.

We find that $\Psi = 25$ is still the model with the lowest χ^2 ($\chi^2 = 0.61$) when the convolved fit procedure is applied to NGC 3379 (data of DC85). The scale ($S = 154''$) is the same as found in § III*c* inside the error δS. The differences between the fit and the data are less than 0.1 mag in all the radial range $R_{min} \leq R \leq R_{max}$. The differences between this fit and that of § III*c* become negligible for $R > R_{min}$. For NGC 7626 (see Fig. 3) we find that $\Psi = 12$ is still the model with the lowest χ^2 ($\chi^2 = 0.19$), with a scale $S = 165''.0$ and differences less than 0.1 mag in all the relevant radial range.

Quite different results are found, as might be expected, when the fit with convolution is applied to King models, which have an intrinsic core structure. For example, the best King model for NGC 4374 (see Fig. 1), when the inner part of the galaxy is included, becomes $C = 2.35$. These tests indeed show that a single King model usually cannot give a reasonable fit to the core and at the same time to the main body of the galaxy. In this sense, we note that King models are best suited for "local" fits in contrast to f_∞-models which usually appear to provide good "global" fits.

We conclude that the convolution does not affect appreciably the choice of the best-fit f_∞-models (the values of Ψ are unchanged and the values of χ^2 are slightly higher than those in § III*c*), that the scales calculated in § III*c* are underestimated by $\sim 1\%$ when the best-fit model exceeds the observed luminosity at $R < R_{min}$ (i.e., for most f_∞-models), and are overestimated by $\sim 10\%$ when the best-fit model is below the observed luminosity at $R < R_{min}$ (i.e., for most King models). As a result, the values of most of the masses calculated from the King models (see Table 5) are expected to be slightly overestimated.

Finally, the data of DV79 on NGC 3379 seem to be complete and accurate enough to justify a full fit from the innermost data points out to 28 mag arcsec^{-2}, i.e., without the restrictions generally adopted in the present paper (see comment on the choice of R_{min} and R_{max} before eq. [6]). A fit with convolution following the procedure described above, after a nine-point smoothing of the data gives the result shown in Figure 4. The differences $\Delta\mu$ between the data and the model are less than 0.2 mag over all the radial range and mostly

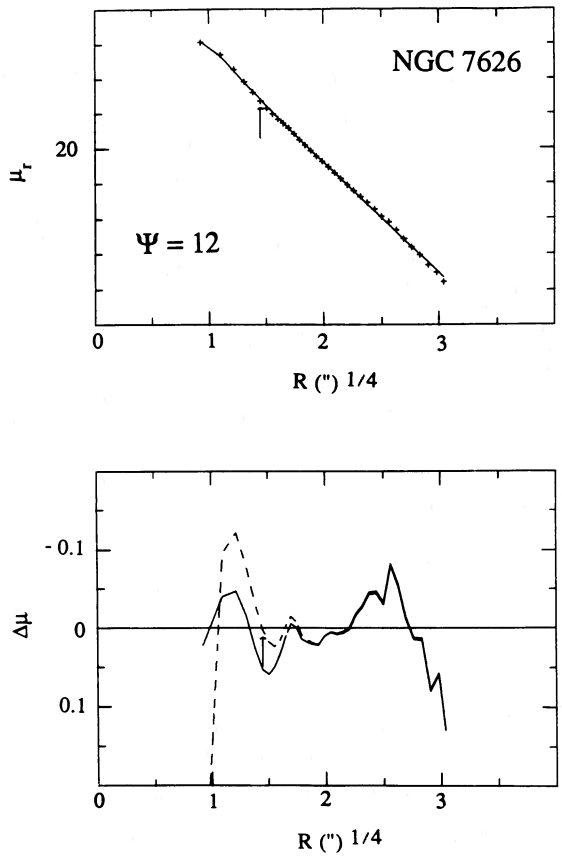

FIG. 3.—For NGC 7626 the convolved photometric fit to the f_∞ models is shown in a format similar to Fig. 2. The differences $\Delta\mu$ between the data and the convolved fit (*solid line*) are less than 0.1 mag. in the whole radial range. The dashed line shows the differences between the data and the unconvolved fit.

confined to ± 0.05 mag, from $R_{\rm min} \approx 6 \times 10^{-4} R_{\rm ef}$ to $R_{\rm max} \approx 7R_{\rm ef}$, with $R_{\rm ef} \approx 63''.1$. This best fit has $\Psi = 12$ and $\chi^2 = 0.7 \pm 0.12$. A similar result is obtained using the PSF described by DV79.

IV. SUMMARY OF THE MAIN RESULTS AND DISCUSSION

a) Photometry

From Table 3 we see that the anisotropic f_∞-models always give the photometric fit with the lowest χ^2, except for two galaxies. For NGC 4374 and NGC 4486 (data from KI78) the King model $C = 2.03$ has the lowest χ^2 and for NGC 4486 (data from DC85 and YW78) the $R^{1/4}$ law gives the best fit. For these less favorable cases, we may note that for NGC 4486 (DC85 and YW78) the performance of the anisotropic f_∞-models is also very good ($\chi^2 = 0.26$), while for NGC 4374 and NGC 4486 (KI78) the fit is over a very small number of data points (see Table 1). In fact, for NGC 4374 the $\Psi = 25$ model gives by far the best fit to the more numerous data of Michard (1985). Regarding the overall quality of the fits, almost all the minimum values of χ^2 are well below unity, as a consequence of our setting $\sigma_m = 0.1$ magnitudes (see § IIIc) which probably overestimates the real errors on the data and possibly because the number of independent data points is likely to be overestimated. As a result, the errors on the parameters of the fit are also likely to be overestimated. These conclusions are illustrated by a comparison of the two different fits on MI85 (see Table 3). Therefore, χ^2 appears to be a good measure of the quality of the fit in order to discriminate various models for a given galaxy. On the other hand, without a more complete analysis of errors, χ^2 may not be an absolute measure of the quality of the fits.

For the photometries without error information, NGC 7626 (data from DC85) has the fit with the lowest χ^2 while NGC 4486 (data from KI78) has the highest. Only in this latter case the best fit model has $\Psi = 6$, all others having $\Psi \geq 9.6$. Imposing the constraint of the total luminosity (eq. [7]) has somewhat tilted the balance of the various fits toward larger values of Ψ. Without such a constraint, many cases would have had the lowest χ^2 corresponding to $\Psi = 7.7$. The errors on Ψ can be very large for $\Psi \geq 25$. This reflects the fact that the anisotropic f_∞-models with high Ψ are very similar to each other.

The fit extends up to $\sim 3R_{\rm ef}$, where $R_{\rm ef}$ is the radius that contains half of the luminosity of the model; $R_{\rm ef}$ is always larger than R_e as calculated from the $R^{1/4}$ fit, although only for NGC 4486 (data from KI78) $R_{\rm ef}$ differs from R_e much more than what would be consistent with the errors on $R_{\rm ef}$. *In the region of the fit* ($R_{\rm min} \leq R \leq R_{\rm max}$) *the differences between the magnitudes of the anisotropic* f_∞*-models and the photometric data are less than 0.15 mag.* At distances $R \leq R_{\rm min}$ from the center, the luminosity of the model *exceeds* the observed luminosity, possibly because the latter is flattened by seeing effects (see the clear example of NGC 7626, shown in Fig. 3).

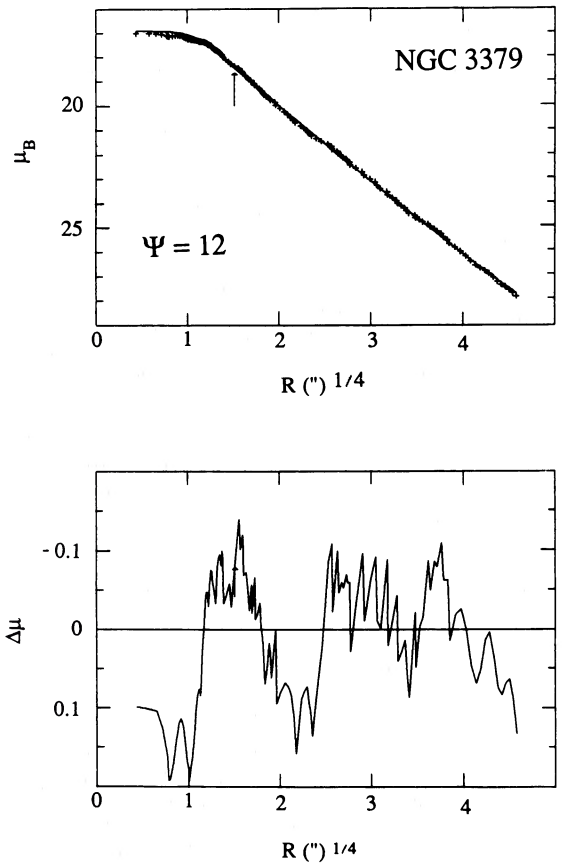

FIG. 4.—The seeing-convolved photometric fit by the f_∞ model $\Psi = 12$ for NGC 3379 is shown in a format similar to Fig. 2. The data, from de Vaucouleurs and Capaccioli (1979), have been reduced with a nine-point smoothing.

(Of course these considerations refer to models that do not possess degenerate cores. The theoretical issue of a degenerate core [see Stiavelli and Bertin 1987] could become an urgent matter if, after seeing convolution [see § III*e*], models like f_∞ still appear brighter than the galaxy in the inner parts.) The only exception is again NGC 4486 (data from KI78), where the model $\Psi = 6$ (a relatively low value for Ψ, the lowest found) is below the observed luminosity. A special comment is required by the E0p galaxy NGC 4486. Even though a good fit to the overall photometry by f_∞-models seems certainly available (see Fig. 1), we should stress that the nuclear structure of this galaxy (see data of YW78, inside $4'' \approx 400$ pc) is clearly beyond the present application of the f_∞-models.

The galaxy NGC 3379 provides the best case for the simple f_∞-models. In fact, given the abundance of accurate data points both in the nuclear region and in the outer parts of the galaxy (DV79), we have extended our analysis so as to obtain a full fit (by a *single* model), and we have obtained very good results (see Fig. 4).

For three galaxies (NGC 3379, NGC 4486, and NGC 7626) we consider photometries in different bands. For NGC 4486 the model with the lowest χ^2 in the B band is $\Psi = 6$ while it is $\Psi = 12$ in the R and V bands. For NGC 7626 the model with the lowest χ^2 is $\Psi = 12$ in the r band and $\Psi = 18$ in the B band. All these facts point to the presence of color gradients in the galaxies (see Boroson and Thompson 1987).

Referring to the King models, the values of the minimum χ^2 obtained from the photometric fit are in the majority of cases at the same time larger than the values of the corresponding values of χ^2 for the f_∞-models and the $R^{1/4}$ law. The galaxy NGC 4472, which was initially thought (KI78 and Kormendy 1982) to be well described by a King model, turns out to have one of the highest value of χ^2. This is in line with the results of Kormendy (1985) and Lauer (1985*b*, p. 109). NGC 7626 (data of KE84) has the lowest χ^2. The best-fit models have usually $C = 2.03$ or 2.35; in two cases $C = 2.69$. In general the luminosities of the King models are below the observed luminosities at distances $R \leq R_{\min}$ from the center. This feature generates sizeable variations of the values of the parameters C and S of the fit when convolution with the seeing is taken into account (see § III*e*). The fit to the photometries in different bands of a given galaxy yields different values of the parameters C and S, as we have already noted for the anisotropic f_∞-models.

b) Kinematics

The kinematical data extend up to a fraction of $R_{\rm ef}$. Only for NGC 3379 do they reach $R_{\rm ef}$. The values of $\chi^2_{\rm kin}$ listed in Table 4 are always near unity (inside the "statistical" error), even for NGC 7619 and NGC 7626, where the velocity dispersion seems to increase at large distance from the center. Therefore we conclude that anisotropic f_∞-models are able to fit at the same time the photometry and the kinematics for the present set of elliptical galaxies. On the other hand, the errors on the kinematical data are so large that from the present kinematical fit alone we cannot exclude that also isotropic distribution functions, like the King models, can be used to fit the velocity dispersion of ellipticals. It is the combined photometric-kinematical fit that definitely favors the anisotropic f_∞-models.

Indeed, the values of $\chi^2_{\rm kin}$ of the kinematical fit based on the King models are near unity, as for the anisotropic f_∞-models, except for the case of NGC 3379 ($\chi^2_{\rm kin} = 2.3$). The values of the projected central velocity dispersion V are systematically 30% smaller than the corresponding values for the anisotropic f_∞-models. This is a consequence of the fact that the King models have a quite flat velocity dispersion profile in the central regions.

The values of the masses derived from the King models are slightly different from those derived from the f_∞-models. Of course, some differences may be expected. However, their significance should be checked against the errors (typically 20% for the f_∞-models) associated with each case. Also we should keep in mind the contribution of specific effects such as the role of the seeing on the scale S of the models (see § III*e*).

c) Mass-to-Light Ratios

In Table 6 for each galaxy (col. [1]) we list the values of M/L_B derived in this paper (cols. [2] and [3]) and those calculated by other authors using different methods. The results of Bacon, Monnet, and Simien (1985, hereafter BM85, col. [4]) were obtained from an application of the virial theorem, those of Lauer (1985*b*, hereafter LA85, col. [5]) from the King core-fitting method and those of Katz and Richstone (1985, hereafter KR85, col. [6]) from an application of linear programming techniques. All the values are scaled to the distances assumed in § III*d*. The differences between the values are partly due to the different values of the central projected velocity dispersion taken by the various authors. The overall agreement between values of M/L_B obtained from *global* methods in this paper and those obtained from *local* methods such as core fitting supports the view that taking an approximately constant M/L ratio is indeed a good assumption.

A first inspection of our results in search for correlations between various quantities has given negative answers. A marginal correlation between M and M/L_B is noted.

d) Conclusion

In conclusion, the very good quality of the fit based on the anisotropic f_∞-models supports the hypothesis that the M/L ratio is approximately constant up to the last points considered. As a result, given the absence of strong color gradients, dark matter is absent, or, at least, approximately distributed like the luminous matter. On the other hand, surprises might be encountered when reliable velocity dispersion data will become available on a larger radial extent, i.e., beyond $R_{\rm ef}$, possibly giving precious information on the existence and extent of dark matter in ellipticals. Therefore one should consider two component models where one is dark and can account for a variable M/L. These models give definite predictions on the gravitational field in the galaxy. Thus a complete fit on objects that include gas rotation curves would be highly desirable.

TABLE 6

MASS-TO-LIGHT RATIOS

Galaxy	f_∞	King	BMS85	LA85	KR85
NGC 3379.....	9.0	10.8	6.1	9.6	...
NGC 4374.....	11.9	12.4	9.6	9.6	9.7–16
NGC 4472.....	6.3	6.5	8.1	11.2	5.4–18
NGC 4486.....	11.1	7.2	11.3	...	...
NGC 4636.....	11.7	15.0	8.4	13.6	10–24
NGC 7562.....	4.6	4.8	7.6	7.4	...
NGC 7619.....	7.3	8.5	8.1	6.4	...
NGC 7626.....	14.4	10.5	8.6	7.4	...

We would like to thank T. van Albada, O. Bendinelli, M. Capaccioli, S. Casertetano, P. Grosbøl, R. Rampazzo, P. Schechter, and S. di Serego Alighieri for useful comments and conversations. Part of this work originated from the Tesi di Laurea of one of us (R. P. S.). Partial support from M.P.I. and C.N.R. of Italy is gratefully acknowledged.

REFERENCES

Bacon, R., Monnet, G., and Simien, F. 1985, *Astr. Ap.*, **152**, 315 (BMS85).
Bendinelli, O., Lorenzutta, S., Parmeggiani, G., and Zavatti, F. 1984, *Astr. Ap.*, **138**, 337.
Bertin, G., and Stiavelli, M. 1984, *Astr. Ap.*, **137**, 26.
———. 1987, in *IAU Symposium 127, Structure and Dynamics of Elliptical Galaxies*, ed. T. de Zeeuw (Dordrecht: Reidel), p. 503.
Bertola, F., Bettoni, D., Danziger, T., Sadler, E., and de Zeeuw, T. 1987, in preparation.
Binney, J. 1982, *Ann. Rev. Astr. Ap.*, **20**, 399.
Boroson, T. A., and Thompson, I. B. 1987, *A.J.*, **92**, 33.
Caldwell, N., Kirshner, R. P., and Richstone, D. O. 1986, *Ap. J.*, **305**, 136.
Capaccioli, M. 1984, *Mem. Soc. Astr. Italiana Suppl.*, **55** (1).
———. 1987, in *IAU Symposium 127, Structure and Dynamics of Elliptical Galaxies*, ed. T. de Zeeuw (Dordrecht: Reidel), p. 47.
Capaccioli, M., and de Vaucouleurs, G. 1983, *Ap. J. Suppl.*, **52**, 465.
Davies, R. L. 1981, *M.N.R.A.S.*, **194**, 879 (DA81).
Davies, R. L., and Illingworth, G. D. 1986, *Ap. J.*, **302**, 234.
Davis, L. E., Cawson, M., Davies, R. L., and Illingworth, G. 1985, *A.J.*, **80**, 169 (DC85).
de Vaucouleurs, G. 1948, *Ann. d'Ap.*, **11**, 247.
de Vaucouleurs, G., and Capaccioli, M. 1979, *Ap. J. Suppl.*, **40**, 699 (DV79).
de Vaucouleurs, G., de Vaucouleurs, A., and Corwin, H. G. 1976, *Second Reference Catalogue of Bright Galaxies* (Austin: University of Texas Press) (RC2).
Dressel, L. 1987, in *IAU Symposium 127, Structure and Dynamics of Elliptical Galaxies*, ed. T. de Zeeuw (Dordrecht: Reidel), p. 423.
Katz, N., and Richstone, D. O. 1985, *Ap. J.*, **296**, 331 (KR85).
Kent, S. M. 1984, *Ap. J. Suppl.*, **56**, 105 (KE84).
King, I. R. 1966, *A.J.*, **71**, 64.
———. 1971, *Pub. A.S.P.*, **83**, 199.
———. 1978, *Ap. J.*, **222**, 1 (KI78).
Kormendy, J. 1977*a*, *Ap. J.*, **214**, 359 (KO77).
———. 1977*b*, *Ap. J.*, **218**, 333.
———. 1982, in *Morphology and Dynamics of Galaxies*, ed. L. Martinet and M. Mayor (Geneva Observatory: Sauverny), p. 113.
———. 1985, *Ap. J. (Letters)*, **292**, L9.
Lauer, T. R. 1985*a*, *Ap. J. Suppl.*, **57**, 473.
———. 1985*b*, *Ap. J.*, **292**, 104 (LA85).
Lynden-Bell, D. 1967, *M.N.R.A.S.*, **136**, 101.
Merritt, D. 1985, *A.J.*, **90**, 1027.
Michard, R. 1985, *Astr. Ap. Suppl. Ser.*, **59**, 205 (MI85).
Mihalas, D., and Binney, J. 1981, *Galactic Astronomy. Structure and Kinematics* (San Francisco: Freeman).
Newton, A. J., and Binney, J. 1984, *M.N.R.A.S.*, **210**, 711.
Pence, W. D., and Davoust, E. 1985, *Astr. Ap. Suppl. Ser.*, **60**, 517.
Raimond, E., Faber, S. M., Gallagher, III, J. S., and Knapp, G. R. 1981, *Ap. J.*, **246**, 708.
Richstone, D. O., and Tremaine, S. D. 1985, *Ap. J.*, **296**, 370.
Rood, H. J., Page, T. L., Kintner, E. C., and King, I. R. 1972, *Ap. J.*, **175**, 627.
Sancisi, R., and van Albada, T. S. 1987, in *IAU Symposium 124, Observational Cosmology* (Dordrecht: Reidel), p. 699.
Sandage, A., and Tamman, G. A. 1981, *A Revised Shapley-Ames Catalog of Bright Galaxies* (Washington, DC: Carnegie Institution of Washington).
Sargent, W. L. W., Young, P. J., Boksenberg, A., Shortridge, K., Lynds, C. R., and Hartwick, F. D. A. 1978, *Ap. J.*, **221**, 731 (SY78).
Schechter, P. L. 1980, *A.J.*, **85**, 801.
Schechter, P. L., and Gunn, J. E. 1979, *Ap. J.*, **229**, 472 (SG79).
Schweizer, F. 1979, *Ap. J.*, **233**, 23.
Shu, F. 1978, *Ap. J.*, **225**, 83.
Stiavelli, M., and Bertin, G. 1985, *M.N.R.A.S.*, **217**, 735.
———. 1987, *M.N.R.A.S.*, **229**, 61.
Thuan, T. X., and Gunn, J. E. 1976, *Pub. A.S.P.*, **88**, 543.
Tremaine, S. 1987, in *IAU Symposium 127, Structure and Dynamics of Elliptical Galaxies*, ed. T. de Zeeuw (Dordrecht: Reidel), p. 367.
Trinchieri, G., Fabbiano, G., and Canizares, C. R. 1986, *Ap. J.*, **310**, 637.
van Albada, T. S. 1982, *M.N.R.A.S.*, **201**, 939.
van Gorkom, J. H., Knapp, G. R., Raimond, E., Faber, S. M., and Gallagher, J. S. 1986, *A.J.*, **91**, 708.
Young, P. J., Westphal, J. A., Kristian, J., Wilson, C. P., and Landauer, F. P. 1978, *Ap. J.*, **221**, 721.

G. BERTIN, R. P. SAGLIA, and M. STIAVELLI: Scuola Normale Superiore—Pisa 56100 I-Italy.